Title

Oxygen dynamics in permafrost thaw lakes: Anaerobic bioreactors in the Canadian subarctic

Journal

Limnology and Oceanography, 60(5)

ISSN

0024-3590

Authors

Deshpande, Bethany N
MacIntyre, Sally
Matveev, Alex
et al.

Publication Date

2015-09-01

DOI

10.1002/lno.10126

Peer reviewed

LIMNOLOGY
and
OCEANOGRAPHY

ASLO

Limnol. Oceanogr. 00, 2015, 1–23

doi: 10.1002/lno.10126

Oxygen dynamics in permafrost thaw lakes: Anaerobic bioreactors in the Canadian subarctic

Bethany N. Deshpande,*[1] Sally MacIntyre,[2] Alex Matveev,[1] Warwick F. Vincent[1]
[1]Centre for Northern Studies (CEN), Takuvik & Biology Department, Université Laval, Québec, Québec, Canada
[2]Department of Ecology, Evolution and Marine Biology, University of California, Santa Barbara, California

Abstract

Permafrost thaw lakes occur in high abundance across the subarctic landscape but little is known about their limnological dynamics. This study was undertaken to evaluate the hourly, seasonal, and depth variations in oxygen concentration in three thaw lakes in northern Quebec, Canada, across contrasting permafrost regimes (isolated, sporadic, and discontinuous). All lakes were well stratified in summer despite their shallow depths (2.7–4.0 m), with hypoxic or anoxic bottom waters. Continuous automated measurements in each of the lakes showed a period of water column oxygenation over several weeks in fall followed by bottom-water anoxia soon after ice-up. Anoxic conditions extended to shallower depths (1 m) over the course of winter, beginning 18–137 d after ice formation, depending on the lake. Full water column anoxia extended over 33–75% of the annual record. There was a brief period of incomplete spring mixing with partial or no reoxygenation of the bottom waters in each lake. Conductivity measurements showed the build-up of solutes in the bottom waters, and the resultant density increase contributed to the resistance to full mixing in spring. These observations indicate the prevalence of stratified conditions throughout most of the year and underscore the importance of the fall mixing period for gas exchange with the atmosphere. Given the long duration of anoxia, subarctic thaw lakes represent an ideal environment for anaerobic processes such as methane production. The intermittent oxygenation also favors intense methanotrophy and aerobic bacterial decomposition processes.

Northern landscapes underlain by permafrost (perennially frozen ground) are currently in rapid transition in response to atmospheric warming (AMAP 2012). The unfrozen surface layer (active layer) has deepened in certain regions, and the vast, ancient reserves of organic carbon stored in the permafrost have begun to be mobilized (Schuur et al. 2015). Considerable research has focused on the influence of climate warming on greenhouse gas emissions from permafrost soils (e.g., McGuire et al. 2012; Elberling et al. 2013), but the lakes on permafrost landscapes and their biogeochemical responses to climate change have only recently begun to receive close attention.

Thaw lakes (thermokarst lakes and ponds) are one of the most abundant freshwater ecosystem types in the circumpolar North, with a likely total area of $2.5–3.8 \times 10^5$ km^2 (Grosse et al. 2013), yet their limnological properties have been little explored. They form when landscape depressions fill with water following thermokarst action: the thawing, collapse and erosion of ice-rich permafrost (Allard and Seguin 1987). The resultant lakes are generally shallow in depth and of limited area, from a few square meters to several square kilometers (Laurion et al. 2010; Grosse et al. 2013), often with high concentrations of dissolved organic carbon (up to 26 mg L^{-1}; Breton et al. 2009). The Downing (2009) scaling equation draws attention to the global importance of small lakes and ponds in general, given their high numerical abundance combined with extreme bioreactivity per unit area; thaw lakes provide an example of this combination of properties, and have been identified as a globally significant source of greenhouse gases (Walter et al. 2006). Small lakes at high northern latitudes dominate the total land-water interface (perimeter) of lakes throughout the world (Verpoorter et al. 2014), and the large total perimeter of eroding permafrost soils that surround northern thaw lakes further indicates their potential biogeochemical significance.

Lakes across the circumpolar North are responding in variable ways to climate warming, with drainage, infilling or evaporation of thaw lakes in some areas, but increases in their abundance and size in others (Vincent et al. 2013). In the subarctic region of eastern Canada, the southern

Additional Supporting Information may be found in the online version of this article

*Correspondence: bethany.deshpande.1@ulaval.ca

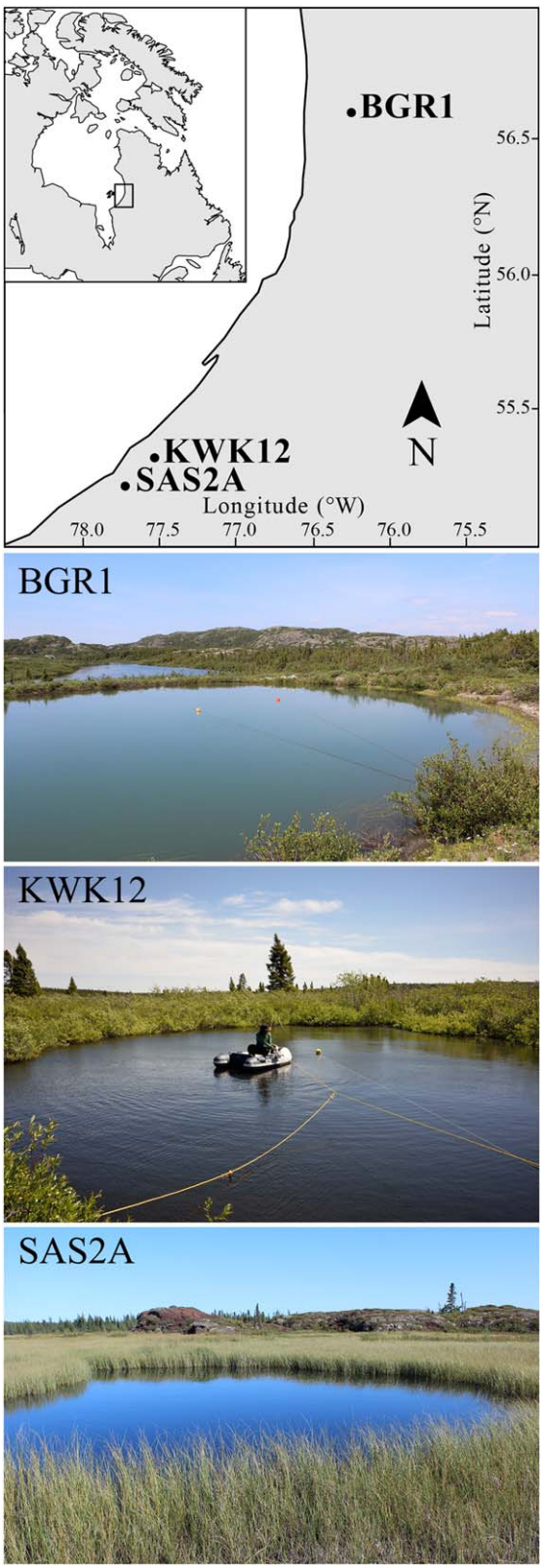

Fig. 1. Location of the three study sites in subarctic Quebec, Canada (top) with photographs of the three thaw lakes.

permafrost limit has moved ~130 km northward over the last three decades, and permafrost thaw lakes in some of this area are expanding (Thibault and Payette 2009). Permafrost thaw ponds in this region are supersaturated in both CO_2 and CH_4 in summer (Breton et al. 2009; Laurion et al. 2010). The bottom waters of these lakes are hypoxic or anoxic during summer, but the seasonal dynamics of oxygen and the duration of anoxic conditions remain unknown. Given that oxygen concentrations determine rates of biogeochemical processes such as methanogenesis, methanotrophy and decomposition of organic carbon to CO_2 (Hutchinson 1957), an improved understanding is needed of how oxygen concentrations vary through time in these waters as well as of the hydrodynamic controls on these variations.

The aim of this study was to determine the oxygen regime of subarctic thaw lakes across a gradient of permafrost conditions, and to evaluate the extent of seasonal variations in anoxia linked to stratification, mixing, and oxygen depletion. We hypothesized that despite the cold, unproductive conditions that normally prevail in northern waters, several conditions would lead to pronounced variations in oxygen concentrations throughout the water column, including summer stratification (Laurion et al. 2010), prolonged ice cover from fall to spring, high organic carbon content for respiration by planktonic bacteria (Breton et al. 2009), and a small ratio of water volume to respiring sediment area. A secondary aim of our study was to define the stratification and mixing dynamics of these waters prior to freezing (ice-on) and immediately after ice-cover melting (ice-off) as critical periods for oxygen and other gas exchanges with the overlying atmosphere. To address these objectives, we sampled three lakes at the southern limit of permafrost in eastern North America, in the subarctic forest tundra-zone (Allard and Seguin 1987). We profiled these remote lakes in summer, and measured oxygen, temperature, and conductivity at hourly intervals throughout an annual cycle using automated in situ sensors.

Methods and materials

Study sites

The three lakes are located near the eastern coast of Hudson Bay in Nunavik, Quebec (Fig. 1) across a gradient of permafrost degradation conditions, from discontinuous (50–90% of the landscape underlain by permafrost) in the North, to sporadic (10–50%) and isolated (< 10%) in the South. BGR1 is a blue-green colored thaw lake in the discontinuous permafrost zone in the Sheldrake River Valley, located 10 km to the northeast of the village of Umiujaq. This valley contains extensive areas of degrading lithalsas (mineral permafrost mounds) and abundant thermokarst lakes (Allard and Seguin 1987; Calmels and Allard 2004). SAS2A is located in the sporadic permafrost zone, in the Sasapimakwananisikw River Valley located 8 km to the south of the contiguous

villages of Whapmagoostui and Kuujjuarapik, and 160 km south of Umiujaq. This water body is one of many black-colored thaw lakes adjacent to rapidly degrading palsas (organic-rich permafrost mounds; Allard and Seguin 1987; Bhiry et al. 2011). KWK12 is a brown-colored lake in a zone of isolated permafrost in the Kwakwatanikapistikw River valley, 110 m above sea level and 12 km to the east of Whapmagoostui-Kuujjuarapik. The KWK valley contains numerous lakes of various colors (Watanabe et al. 2011) that have been derived from fully thawed lithalsas, with extensive tree and shrub development around the lakes. Over 95% of the permafrost mounds in this valley thawed and disappeared between 1959 and 2006, and forest vegetation (black spruce trees) expanded by 326% during this same period (Bouchard et al. 2014).

Lake sampling and profiling

BGR1 was visited once in 2011 and all three lakes were visited once the following three consecutive summers, in 2012, 2013, and 2014; access to these remote sites was by helicopter based out of the CEN field station at Whapmagoostui-Kuujjuarapik. At each visit, temperature, oxygen, pH, and conductivity were measured using a Hydrolab DS5X profiler (Loveland, Colorado, USA). Transparency was measured with a 25-cm black and white Secchi disk. Photosynthetically active radiation (PAR) was measured using an LI-192 radiometer throughout the water column (LI-COR, Nebraska, USA). Near-surface water samples were collected with a Van Dorn water bottle in the pelagic zone at the site of maximal depth and were analysed following Laurion et al. (2010) for total phosphorus (TP), dissolved organic carbon (DOC), chlorophyll *a* (Chl *a*), and total suspended solids (TSS). Dissolved methane and dissolved carbon dioxide were determined via the headspace method. Major ions were determined by ion chromatography (Dionex ICS 2000) for anions, and via atomic emission spectroscopy (Varian Vista AX) for cations; bicarbonate concentrations were determined from pH and ion balance calculations.

Automated in situ measurements

Mooring systems for the three lakes were constructed with metal chain and a surface buoy to keep the chain upright, a floater part way down the chain to reduce within-lake displacement, and a bottom weight resting on the sediments. The systems were secured to opposite ends of each lake using low-stretch rope. The following sensors were affixed to the chains by tie-wraps: dissolved oxygen and temperature loggers (DOT: MiniDO$_2$T optode systems, Precision Engineering, California, USA; oxygen resolution: 1.6 μg L^{-1}, temperature resolution: 0.01°C); conductivity and temperature loggers (CT: Hobo U24-001, Onset Computer Corporation, Massachusetts, USA; conductivity resolution: 1.0 μS cm^{-1}, temperature resolution: 0.01°C); and additional temperature loggers (T: Minilog-II-T; VEMCO/Amirix Systems, Nova Scotia, Canada; T resolution: 0.01°C). The configurations for each lake were determined according to the summer water column profiles, the availability of loggers and to minimize freezing of the sensors. Previous data logger measurements suggested an overwinter ice thickness up to 0.6 m. For the BGR1 deployment (19 August 2012 to 04 July 2013), the loggers were installed at 0.7 (T), 1.0 (DOT), 1.5 (T), 2.0 (DOT and CT), 2.5 (T), and 3.5 m (DOT and CT). For the KWK12 deployment (20 August 2013 to 25 June 2014), the loggers were installed at 1.0 (DOT), 2.0 (T) and 2.5 m (DOT), and for the SAS2A deployment (19 August 2013 to 25 June 2014) at 0.6 (CT), 1.0 (DOT), 1.55 (T), 2.05 (T), and 2.7 m (CT). The optode (DOT) and conductivity (CT) sensors were set to a logging frequency of 60 min, and the temperature sensors (T) were set to 15 min. For the BGR deployment, the optodes were installed in the lake with protective, low density, polyethylene caps, and for KWK12 and SAS2A they were installed without the caps. Oxygen sensors were tested with and without caps in the laboratory to check porosity to oxygen and gave values within ± 4.7% of each other. The prospect of biofouling of the sensors was a consideration, since these instruments do not have a mechanical wiper. There was no visible growth over the sensors with or without the caps, although a thin smooth film was apparent by touch. The recovery of all sensors to 80–100% oxygen readings during mixing and reoxygenation events in the lakes or immediately after their transfer from anoxic water to the air also suggests that any biofilm had minimal effect on the in situ oxygen readings.

Water column stability

Calculations of density and Wedderburn number were made for BGR1, for which there were continuous records of conductivity at two depths. The density (ρ) of the water was calculated separately based on temperature and temperature plus salinity using a nonlinear equation of state for freshwaters (Chen and Millero 1977). For temperature-based density, the salinity terms were set to 0. For temperature- and salinity-based density, a conversion factor of 0.8 times the specific conductivity was determined based on the major ion content (including bicarbonate) of the thaw lake waters; this conversion factor falls within the range 0.6–0.9 as determined in other studies (Pawlowicz 2008). The average conductivity measured in summer 2012 and 2013 was used as a reference value for conductivity in the surface layer. The Wedderburn number, an index of water column stability and a guide to whether upwelling and mixing in the water column are induced by internal wave motions, was calculated as in Imberger and Patterson (1990):

$$W = \frac{g' \cdot h_{\mathrm{m}}^2}{u_{*w}^2 \cdot L} \tag{1}$$

where $g' = g\ (\Delta\rho/\rho_{\mathrm{avg}})$ is the effective gravity related to the density difference across the mixed layer, h_{m} is the depth of the surface mixed layer, L is the fetch, and $u_{*\mathrm{w}}$ is the water

friction velocity derived from shear stress, assuming it is equal on both sides of the air-water interface. The drag coefficient and law of the wall scaling follow Amorocho and DeVries (1980). Density was calculated as described above.

The period of first mode internal waves (T) was calculated as in Kalff (2002):

$$T = \frac{2L}{\sqrt{g(\rho_h - \rho_e)/\left(\frac{\rho_h}{z_h} + \frac{\rho_e}{z_e}\right)}} \quad (2)$$

where L is fetch, ρ_h is the density of the hypolimnion, ρ_e is the density of the epilimnion, z_h is the depth of the hypolimnion, and z_e is the depth of the epilimnion.

Oxygen depletion rates

Rates of oxygen loss after the onset of ice cover were calculated by linear regressions of oxygen concentrations vs. time (SigmaPlot 11.0). Visual inspection of the graphs indicated a break in slopes for some of the measurements, and therefore the early and late parts of the oxygen depletion curve were treated separately.

Results

Limnological properties and greenhouse gas concentrations

All of the lakes in summer had low concentrations of phytoplankton in their surface waters, with Chl *a* concentrations up to 2.0 μg L^{-1} (Table 1). Total phosphorus levels were in the range 22–32 μg L^{-1}, while dissolved organic carbon concentrations varied from 3 to 15 mg L^{-1}, with highest values in SAS2A. Total suspended solids varied from 1 to 5 mg L^{-1}, with highest concentrations in the brown turbid waters of KWK12. The Secchi disk transparency of the lakes was similarly variable, ranging from 0.6 m in DOC-rich SAS2A to 3.5 m in the blue-green waters of BGR1. The surface waters of all three lakes had greenhouse gas concentrations that were supersaturated relative to air, with maximum values in SAS2A that were one (CO_2) or five (CH_4) orders of magnitude above atmospheric-equilibrium values. These high concentrations indicate the lakes were net heterotrophic with potential for strong emissions of both gases, and especially methane, to the atmosphere.

Table 1. Limnological properties of the three thaw lakes in August 2013. The CO_2 and CH_4 gas saturation values are % of gas values in water that is in equilibrium with air (19.5 μmol CO_2 L^{-1} and 0.0034 μmol CH_4 L^{-1}; Laurion et al. 2010)

Variable	BGR1	SAS2A	KWK12
GPS location			
Latitude N	56° 37′	55° 14′	55° 18′
Longitude W	76° 13′	77° 42′	77° 30′
Width (m)	30	14	18
Length (m)	41	21	29
Depth (m)	4.0	2.7	2.7
TSS (mg L^{-1})	1.59	0.96	4.58
POC (mg L^{-1})	1.29	1.56	3.93
Secchi (m)	3.5	0.6	1.5
TP (μg L^{-1})	22.2	26.3	31.9
Chl *a* (μg L^{-1})	0.93	1.90	0.28
DOC (mg L^{-1})	2.7	14.8	6.5
CO_2			
μmol L^{-1}	22.6	389.7	43.7
% saturation	116	1998	224
CH_4			
μmol L^{-1}	1.09	2.16	0.17
% saturation	31969	63567	4892

Summer lake profiles

BGR1, the deepest and most northerly lake of our study, had a maximum depth of 4.0 m in summer 2013 (Table 1). The summer water column temperatures dropped almost linearly from 20.0°C at the surface to 9.5°C at the bottom (Fig. 2). Specific conductivity in BGR averaged (SD) 94 (4) μS cm^{-1} throughout the upper 3 m of the lake, and in the bottom waters rose to a maximum of 220 μS cm^{-1}. The concentrations of dissolved oxygen remained above 100% saturation for most of the upper 3 m, and over the bottom meter dropped rapidly from 90% to 25% saturation. Summer profiling of SAS2A in 2014 showed that temperatures dropped from 13.9°C at the surface to 3.7°C at a depth of 2.3 m with stratification most pronounced in the upper 0.75 m (Fig. 2). Conductivity was relatively constant over the upper 0.5 m of the water column, and then rose to a maximum of 209 μS cm^{-1} at the bottom. Oxygen was near-saturation at the surface (118%) and declined rapidly to 0% at 0.35 m and below. Water column profiling of KWK12 in summer 2014 (Fig. 2) showed that temperatures dropped from 18.5°C at the surface to 6.4°C at 2.2 m with two step-like features indicating multiple thermoclines. Specific conductivity increased over the bottom 1 m of the profile to a maximum of 57 μS cm^{-1}. Dissolved oxygen ranged from supersaturated at the surface (139%) and decreased through the water column to 0% at 1.5 m and below. The largest increases in specific conductivity and decreases in oxygen occurred below the second thermocline. Radiometric profiles (not shown) gave estimated euphotic depths (depth of 1% surface PAR) of 2.0 m for KWK12, and 0.8 m for SAS2A. The euphotic depth for BGR1 was greater than the maximum depth of this lake, where irradiance was 6% of surface PAR.

Seasonal variations in BGR1

The water column was well stratified in late summer, and underwent cooling and mixing from mid-September to late October (Fig. 3). In October, the lake cooled to 2°C, warmed to 4°C and then developed inverse stratification under the ice, which persisted until late May. From mid-November

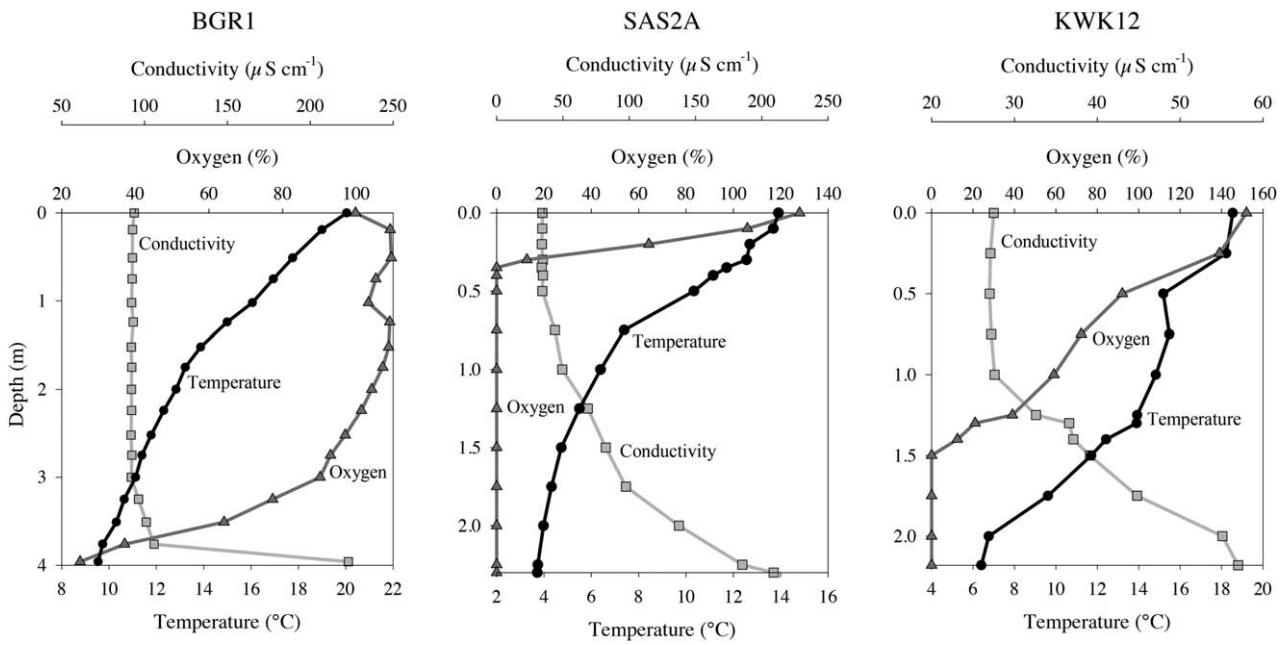

Fig. 2. Water column profiles of temperature, specific conductivity, and oxygen in the three thaw lakes. The dates of sampling were 31 July 2013 (BGR1), 26 June 2014 (SAS2A), and 26 June 2014 (KWK12).

onwards, temperatures at 3.5 m decreased more than those at 2.5 m, and there was a mid-water column maximum that was up to 0.6°C warmer than near bottom temperatures. Thermal stratification was weakest at the end of May and the beginning of June, with the onset of warming. Temperatures did not become uniform, indicating that the full water column did not mix in spring; the stratification at that time was enhanced by salinity which increased over the course of winter (Fig. 4) and contributed to the density gradient within the water column (Supporting Information Fig. S1). Once warming began, diurnal heating and cooling was constrained to depths between 0.5 m and 0.75 m, with more consistent heating at 1 m. Warm water was mixed downwards discontinuously, penetrating to 2.5 m by 7 June and to 3.5 m by 23 June. The concomitant near-surface cooling suggests the mixing was mediated by the passage of a cold front. The abrupt decrease in temperature in the upper 2 sensors and the increase in the bottom sensor on 23 June followed by a near return to the original values indicates wind induced thermocline tilting.

The pattern of stratification and mixing in BGR1 was further shown by the conductivity and temperature records near the bottom of the lake (Fig. 4). The bottom water temperatures of BGR1 were above 10°C until mid-September, and then fell in a series of steps to around 2°C in mid-October. The thermistor in the surface sediments at the edge of BGR1 first showed temperatures below zero on 16 October, implying ice-up at that time. From mid-October to mid-November the bottom waters warmed to 4°C. The conductivity probes showed a difference of around 25 μS cm^{-1} between 2 m and 3.5 m during late August stratification. This difference lessened and the readings intersected in value several times until mid-October, indicative of water column mixing during this period of fall cooling. There was a marked increase in conductivity at both depths during winter, with a much greater increase at 3.5 m, where values ultimately rose to 423 μS cm^{-1}. Over the winter, the increased specific conductivity caused a minor increase in density relative to that from temperature alone at 2 m depth but increased the density by 2 kg m^{-3} above that expected from temperature alone at 3.5 m; this effect was reduced but persisted throughout summer (Supporting Information Fig. S1). Conductivities as well as computed densities began to drop on 07 May, implying ice-out and the onset of mixing; however the 2.0 m and 3.5 m values for both variables did not intersect even when water temperatures became near uniform on 23 June, indicating only partial mixing in spring. Based on temperature alone, the density of the lake is such that it would have mixed under the ice. The increased density from the salts accumulated in the bottom waters over the winter maintained stable stratification and created the observed resistance to mixing in spring.

Maximum dissolved oxygen values were observed in BGR1 at the beginning of the continuous record (18 August 2012), with near saturation values in the surface (103.1%) and middle (99.5%) waters, dropping to 74.3% at the bottom of the water column (Fig. 4). Bottom water values decreased over the subsequent 3 weeks, with a brief spike at the end of August. This was associated with an episode of high winds that peaked at 12.9 m s^{-1} (46 km h^{-1}) at Umiujaq on 28

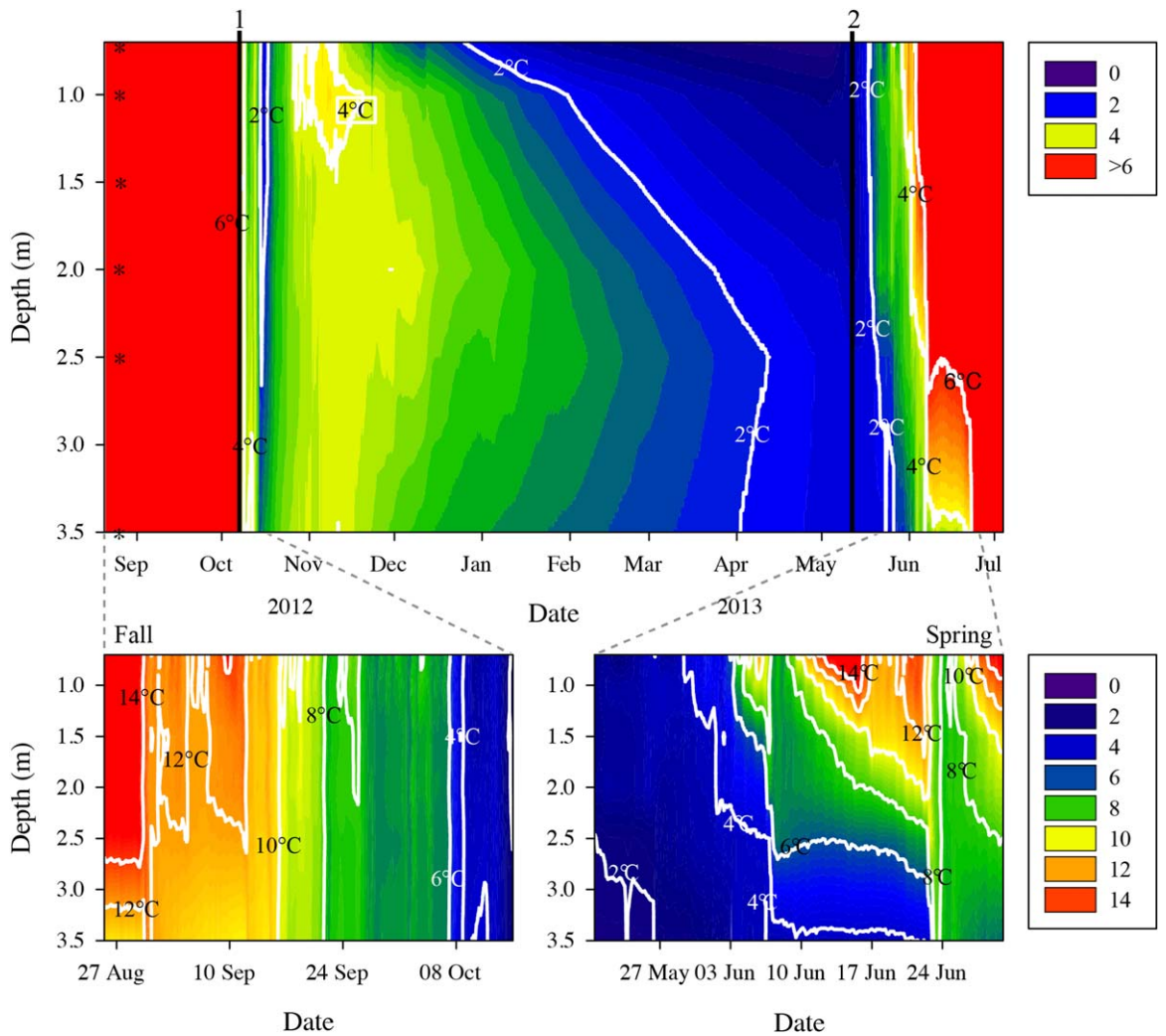

Fig. 3. Temperature variations in the water column of BGR1 from August 2012 to July 2013. The isotherms (white lines) are at 2.0 °C intervals. Asterisks on the upper panel *y*-axis correspond to logger depths. The lower left panel shows the fall period from 25 August to 15 October 2012. The lower right panel shows the spring period from 20 May to 30 June 2013. Vertical lines show (1) the beginning of ice-formation in autumn, and (2) the beginning of spring thaw, as indicated by an air temperature threshold of 24 h below or above 0 °C.

August 2012 (CEN 2014a), and corresponded to sudden drops in BGR1 water temperatures at 1 m and 2 m, and a peak in temperature at 3.5 m. The bottom water oxygen rose from a minimum of 15% in September to a maximum of around 80% in mid-October (from 1.6 to 10.8 mg L^{-1}), consistent with mixing and entrainment of surface waters during that time. Oxygen concentrations then declined to zero over the subsequent weeks, with anoxia occurring first at 3.5, then 2.0 and finally 1.0 m. The anoxic conditions persisted at all depths until an increase in oxygen at 1.0 m in late May and at 2.0 m in June, to maxima of 88% and 70% of saturation (respectively, 9.4 and 7.7 mg L^{-1}) by early July. The 3.5 m record showed only a brief rise in oxygen in late June, to a maximum value of 27.5% saturation (3.4 mg L^{-1}), associated with a mixing event; maximum winds at that time peaked at 12.7 m s^{-1} at the Umiujaq station (20 June 2013; CEN 2014a). Mixing was also indicated by the abrupt rise in water temperature at 3.5 m, the sharp drops in water temperature at 1 m and 2 m, and the abrupt decrease in conductivity at 3.5 m. However, mixing was not complete since the surface vs. bottom differences in oxygen concentration indicate that the water column was not homogenized.

Wedderburn numbers decreased progressively from August until ice-on with values frequently dropping below 1, indicative of considerable internal wave tilting and mixing due to the breaking of nonlinear waves (MacIntyre et al. 2009). Similarly, Wedderburn numbers were also low from ice-off until early June. The frequent abrupt changes in temperature in fall as well as the large jumps in conductivity in spring at 2 m and 3.5 m suggest that internal wave motions

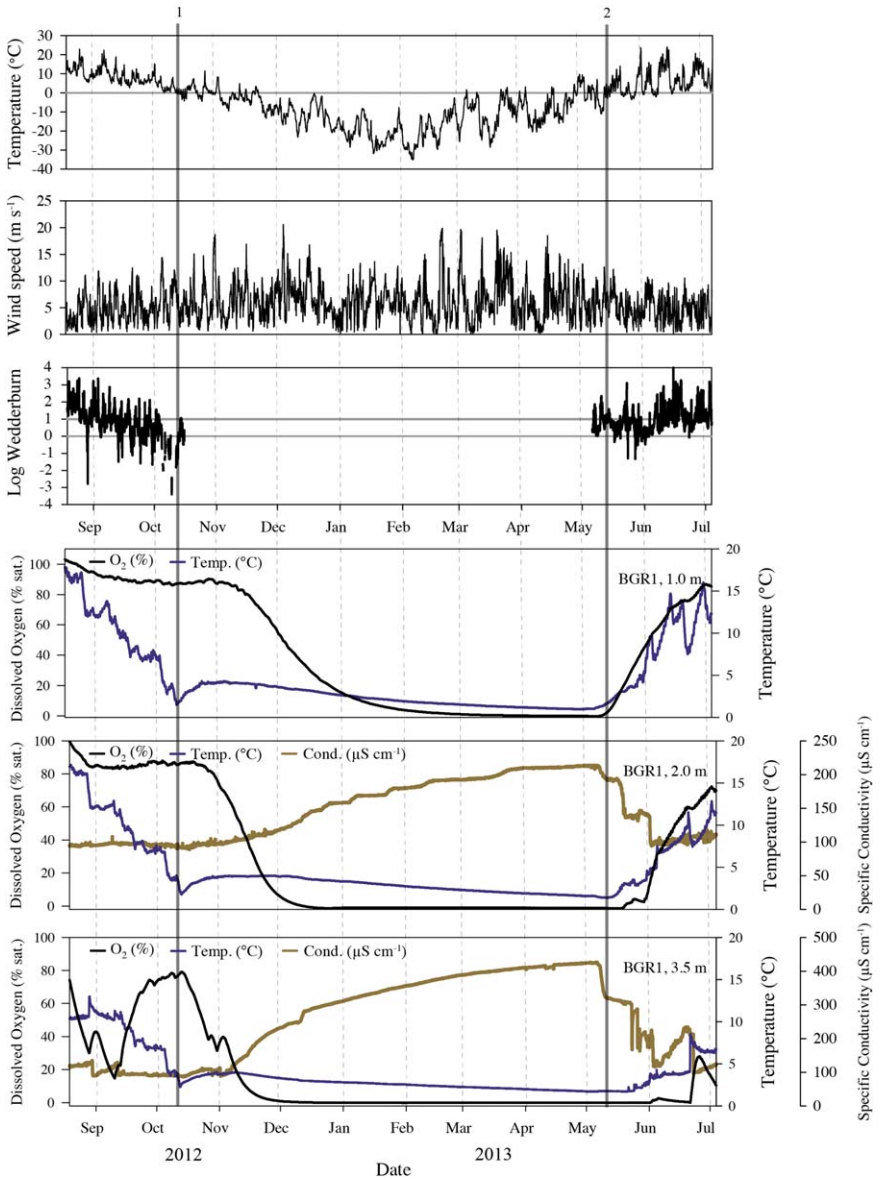

Fig. 4. Seasonal variations in oxygen, conductivity and temperature in BGR1 from 2012 to 2013. Wind speed and air temperature show the annual variations at the nearest meteorological station (Umiujaq; CEN 2014a). Vertical lines show (1) the beginning of ice-formation in autumn, and (2) the beginning of spring thaw, as indicated by an air temperature threshold of 24 h below or above 0 °C.

contributed to the mixing that led to cooling in fall and to the observed decreases in conductivity at the deeper locations in spring.

Seasonal variations in SAS2A

The thermal structure from fall through spring in SAS2A had many similarities to that of BGR1 despite its shallower depth (Supporting Information Fig. S2). However, there were a number of conspicuous differences: the deepest temperatures shortly after ice-on exceeded 5°C, which is unusual given that 4°C is the maximum density of freshwater; there was no mid-water thermal maximum; temperatures decreased more rapidly over the winter; and the full water column became isothermal at 4°C around 22 May, which implies convective mixing at that time.

Only a single oxygen optode was available for the mooring in SAS2A. We installed it along with a conductivity logger at 1 m where the lake was anoxic in summer (Figs. 2, 5). Anoxia at this depth continued until early September, after which there was a 6-week period of mixing and entrainment of oxygenated waters, to a maximum of 45% saturation (5.5 mg L^{-1}) in late September. Oxygen concentrations fell from mid-October onwards and at faster rates over the last days of October, to anoxia by the beginning of November.

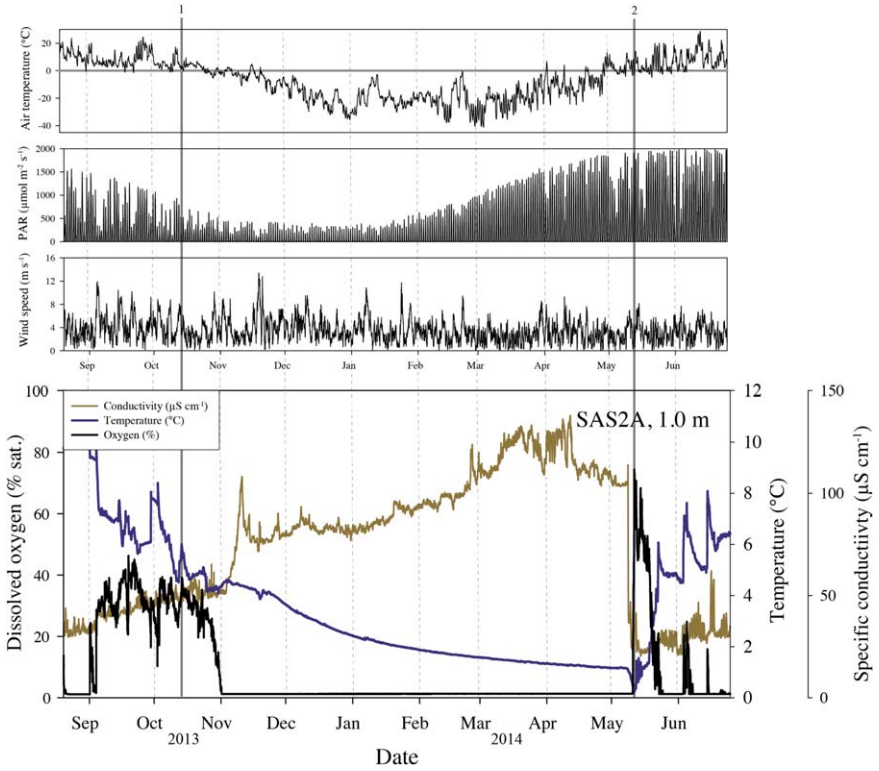

Fig. 5. Seasonal variations in oxygen, conductivity, and temperature at 1.0 m in SAS2A from 2013 to 2014. The annual record of air temperature, incident PAR irradiance, and wind speed are from the nearest meteorological station (Whapmagoostui-Kuujjuarapik; CEN 2014b). Vertical lines show (1) the beginning of ice-formation in autumn, and (2) the beginning of spring thaw, as indicated by an air temperature threshold of 24 h below or above 0 °C.

Anoxia then persisted at this depth until a series of three mixing events, with the largest in mid-May that increased oxygen concentrations to just below 75% saturation (10.7 mg L^{-1}). This event was induced by increased winds. The subsequent two mixing events, also evident in the temperature record, increased oxygen to less than 25%, and in all cases, anoxia was rapidly re-established within a few days.

Specific conductivity gradually increased from September until November. This increase was likely due to mixing with the waters below. The increase in specific conductivity during the period of ice cover was marked by a number of abrupt increases and usually more subtle decreases which often co-occurred with increases in wind. These changes are likely due to internal waves induced by the pressure of wind on the ice (Kirillin et al. 2012). The decrease in specific conductivity in early April was likely due to some downward mixing of fresher water above made possible by instabilities due to increased solar heating. The abrupt increase in oxygen at ice off occurred coincidentally with a decrease in specific conductivity to values less than those in late summer the previous year. These changes occurred coincidentally with high winds during sunny conditions, water temperatures below 4°C, and rapid oscillations in temperature. These combined factors imply internal wave induced mixing at ice off rather than convective mixing. The subsequent oscillations in specific conductivity also co-occurred with the swings in oxygen and temperature. Again, these changes imply internal wave activity at the depth of the sondes.

The conductivity probe at the bottom of SAS2A (2.5 m, data not shown) showed high values during late summer stratification. Beginning in early September, eight mixing events can be identified by sharp decreases in conductivity that were likely the result of entrainment of fresher waters from higher in the water column (Fig. 5). The initial mixing event was associated with warmer temperatures, suggesting wind-induced mixing, while later events were associated with short-term cooling that indicated convective mixing, all superimposed on an overall cooling trend to less than 5°C by the end of November. From mid-October to late December, there was an increase in bottom water conductivity, likely associated with freeze-up, eventually reaching values that were five times those measured during summer. From January onward this 2.5 m conductivity probe registered falling readings that eventually became negative, implying instrument malfunction.

Seasonal and diurnal variations in KWK12

As at the other two sites, KWK12 was stratified in late summer, underwent cooling and mixing from mid-

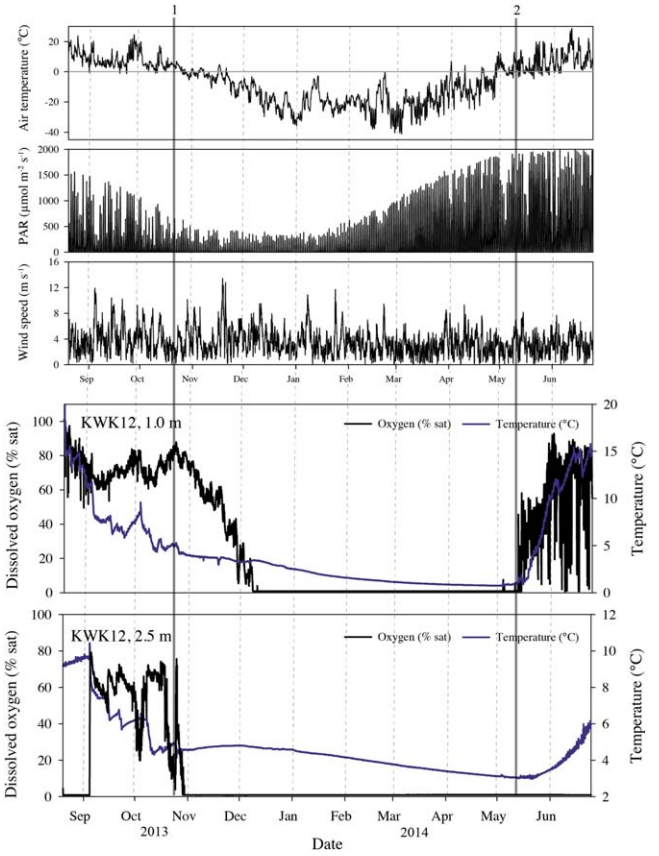

Fig. 6. Seasonal variations in oxygen and temperature at two depths in KWK12, 2013–2014, along with annual records of air temperature, wind speed, and incident PAR irradiance at the nearest meteorological station (Whapmagoostui-Kuujjuarapik; CEN 2014b). Vertical lines show (1) the beginning of ice-formation in autumn, and (2) the beginning of spring thaw, as indicated by an air temperature threshold of 24 h below or above 0 °C.

September to late October, and was inversely stratified under the ice (Supporting Information Fig. S3). There was a brief warming episode in October, as was also observed in SAS2A, and water temperatures below 2 m exceeded 4°C for about 2 months after ice-on (Fig. 6). Warming and mixing occurred in early June, with the establishment of a deeper epilimnion in comparison with SAS2A.

Percent oxygen saturation at 1.0 m in KWK12 showed rapid fluctuations from the start of sampling until anoxia set in after ice-on. Initially saturation was near 100%, then varied within the range 60–80% (7.2–9.6 mg L^{-1}) until late October, and declined after ice on, reaching anoxia by 07 December, 2013 (Fig. 6). Anoxic conditions persisted for 5 months at this depth, and from mid-May onward, oxygen began to rise. There were striking diurnal fluctuations that ranged from 80% saturation during the day to anoxic or hypoxic conditions during the night (Figs. 6, 7). Autocorrelation analysis for this 5-d period showed that wind speed, solar radiation, air temperature and oxygen concentration measured at a depth of 1 m all fluctuated in tandem with a period of 24 h. In the bottom waters of the lake (2.5 m), conditions were initially anoxic in August 2013, and then rose abruptly in early September during a period of high winds (peak mean hourly velocity was 11.9 m s^{-1} on 04 September 2013, Kuujjuarapik; CEN 2014b). There was a series of events with rapid decreases followed by increases in saturation, with the last episode on 25 October. Since the oxygen concentrations returned to previous values, the events are indicative of internal wave motions, not mixing. After ice-on, saturation rapidly decreased and the water was anoxic by 29 October 2013. Anoxic conditions then persisted for the following 8 months. There was no evidence of reoxygenation of these bottom waters in spring 2014, however when the oxygen probe was recovered at the end of the deployment and returned to the surface, measured oxygen concentrations increased to 97.5% saturation, confirming that the sensor was still fully operational.

Oxygen depletion rates

The oxygen loss during early winter was approximated by a linear model in each lake (Table 2). The rates varied among lakes and depths, with most values in the range of 0.1-0.5 mg L^{-1} d^{-1}. Oxygen depletion rates were converted to g O_2 m^{-2} d^{-1} via bathymetric information (V. Proult, Université Laval, unpubl. data). Winter oxygen depletion rates range from a minimum of 0.07 g O_2 m^{-2} d^{-1} in SAS2A to a maximum of 1.33 g O_2 m^{-2} d^{-1} in KWK12, with an average (SD) of 0.45 (0.36) g O_2 m^{-2} d^{-1}. Net oxygen depletion in BGR1 increased with depth, with rates in the bottom waters that were about double those at 1.0 m. In SAS2A at 1.0 m, there appeared to be two linear phases, with initial depletion rates that were about half of those in the second phase. Two phases were also apparent in KWK12 at 1.0 m, which also showed a doubling of rates in the second phase. KWK12 at 2.5 m experienced unusually high rates of short-term oxygen decrease during the depletion events in late October that were 2–100 times faster than in the other lakes and depths. As these were attributed to internal wave induced oscillations, not respiration, we did not include them in the table.

Rapid changes in oxygen also occurred in spring. Based on averaging the five diurnal curves in Fig. 7, average ($\pm$SD) oxygen rose at a rate of 1.22 ($\pm$0.89) mg O_2 L^{-1} min^{-1} and declined at a rate of 0.417 ($\pm$0.248) mg O_2 L^{-1} min^{-1}. These rates are far in excess of respiration rates (Table 2) and expected rates of photosynthesis, and due to the correlated temporal changes in temperature and wind speed, they are likely due to internal waves.

Discussion

The most distinctive feature of the permafrost thaw lakes observed in this study was their rapid drawdown of oxygen once ice cover was established, followed by full water column anoxia that persisted throughout more than 6 months

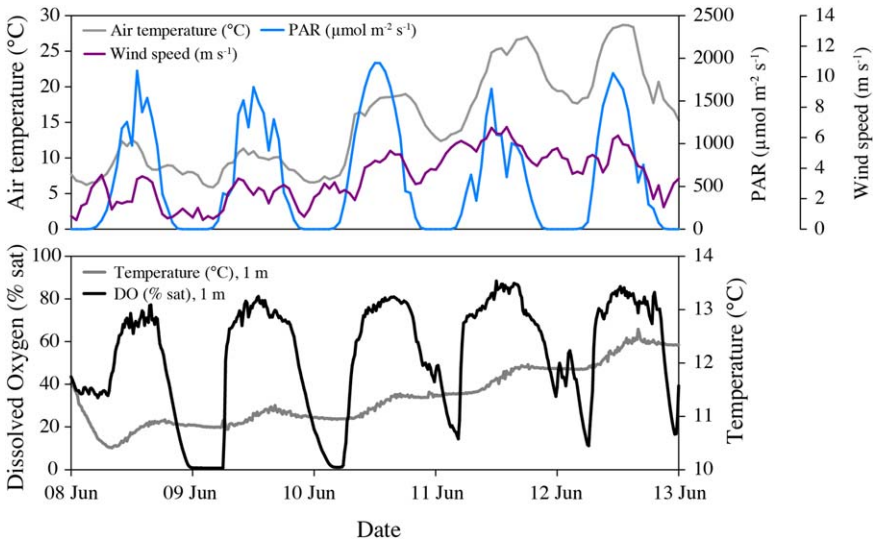

Fig. 7. Diurnal variations in oxygen and water temperature at 1.0 m in KWK12 and air temperature, wind speed, and incident PAR irradiance at the nearest meteorological station (Whapmagoostui-Kuujjuarapik; CEN 2014b) throughout a 5-d period, from 08 June to 13 June 2014.

of winter ice-cover. This contrasts with deeper lakes that have been studied to date in the Arctic. For example, in Char Lake ($Z_{max} = 27.5$ m) in High Arctic Canada, oxygen remained in the range 14–14.5 mg L^{-1} at 10 m throughout 10 months of ice cover, and the observed minimum at the end of winter was 2.5 mg L^{-1} at 26 m (Schindler et al. 1974). At Toolik Lake ($Z_{max} = 25$ m) in northern Alaska, measurements in mid-winter showed oxygen concentrations in the range 8–12 mg L^{-1} throughout the upper water column, to the maximum sampled depth of 16 m (Whalen and Cornwell 1985). In the bottom waters of the subarctic thaw lakes, low or negligible oxygen conditions persisted throughout spring because mixing was intermittent and incomplete, and unlike dimictic lakes studied elsewhere, there was no full water column reoxygenation at that time (Figs. 4-6). Longer, more complete mixing occurred during fall; this season was the most important for water column reoxygenation, and was likely accompanied by ventilation of greenhouse gases to the atmosphere. Below we evaluate the limnological factors and processes that contribute to these distinctive properties of thaw lake ecosystems.

Variability in oxygen concentrations

Consistent with the hypothesis of pronounced variations in oxygen concentration, the three thaw lakes showed large fluctuations throughout the annual cycle, ranging from above saturation to full water-column anoxia. Despite their shallow depths and exposed locations in open landscapes, all three lakes were highly stratified in summer. For example, SAS2A and KWK12 had super-saturated surface waters but anoxic bottom waters during summer sampling (Fig. 2). Summer time oxygen distributions depended on light penetration and the depth of the euphotic zone with some dependence on thermal structure in KWK12 and SAS2A, the two less-transparent lakes. The continuous optode records at all depths had periods in which oxygen exceeded 50%

Table 2. Rates of oxygen decrease in the three subarctic thaw lakes during early winter. $p < 0.001$ for the oxygen vs. time regressions for all rates

Lake	Depth (m)	Start	End	R^2	n	Rate (mg O_2 L^{-1} d^{-1})	Rate (g O_2 m^{-2} d^{-1})
KWK12	1	22 Oct 2013	15 Nov 2013	0.857	2304	0.177	0.22
KWK12	1	16 Nov 2013	07 Dec 2013	0.842	2016	0.332	0.42
KWK12	2.5	25 Oct 2013	30 Oct 2013	0.935	494	1.060	1.33
SAS2A	1	26 Oct 2013	31 Oct 2013	0.936	576	0.498	0.41
BGR1	1	16 Nov 2012	13 Dec 2012	0.997	672	0.223	0.25
BGR1	2	02 Nov 2012	18 Nov 2012	0.995	408	0.355	0.40
BGR1	3.5	14 Oct 2012	24 Oct 2012	0.996	264	0.437	0.49
BGR1	3.5	04 Nov 2012	11 Nov 2012	0.988	192	0.425	0.48

saturation and at other times showed anoxia, but the duration of each of these conditions differed markedly among lakes and depths.

These high-amplitude variations would not be expected in polar and alpine lakes where low temperatures and nutrient concentrations restrict biological processes, and they have not been observed in the oligotrophic lakes and ponds that have been traditionally studied in the Arctic. With the exception of oxygen subsaturation observed during summer in some tundra ponds at Barrow, Alaska (Hobbie 1980), previous observations of Arctic lakes have shown that oxygen remains at full saturation during the open, ice-free period, similar to oligotrophic temperate lakes (Welch 1974; Hobbie 1980; Kirillin et al. 2012).

Oxygen depletion rates

Volumetric oxygen depletion rates during winter were in the range 0.2–1.1 mg O_2 L^{-1} d^{-1} (Table 2). These rates are above those for large, oligotrophic Arctic lakes. For example, oxygen concentrations in Char Lake showed little change over winter through most of the water column, with loss rates at the bottom of the water column in the first 40 d after ice-on at around 0.1 mg O_2 L^{-1} d^{-1} (from Fig. 8 in Schindler et al. 1974). In the subarctic thaw lakes, we observed the highest rates of oxygen depletion near the lake bottom; this may reflect increased organic particle accumulation at depth and richer sediments, but may also be affected by hypoxic water transported from elsewhere. The high respiration rate at depth in KWK12 may have been confounded with an initial internal wave motion that accentuated the rate of decrease.

Per unit area, the oxygen depletion rates in the subarctic lakes were mostly in the range 0.2–0.5 g O_2 m^{-2} d^{-1}; these are similar to under-ice, winter loss rates measured elsewhere; for example 0.1–0.4 g O_2 m^{-2} d^{-1} in lakes in north temperate Ontario (Welch et al. 1976; Welch and Bergmann 1985a) and in an Arctic tundra pond (Ramlal et al. 1994). However, a distinguishing feature of permafrost thaw lakes is their shallow liquid water depth, reduced even further by thick ice formation during winter; these oxygen loss rates are expressed though a short water column, rapidly leading to complete anoxia.

Anoxic water columns under the ice have been reported in shallow lakes elsewhere, with different types of organic matter fueling the respiratory oxygen demand. In eutrophic waters, the decomposition of algal biomass may lead to rapid rates of oxygen depletion; for example in hypereutrophic prairie lakes, oxygen dropped to 1 mg L^{-1}, within a month of ice-on, followed by 4 months of anoxia (Baird et al. 1987). Less eutrophic prairie pothole lakes had a slower rate of oxygen depletion and shorter duration of anoxia (Barica and Mathias 1979). The subarctic thaw lakes lacked these large standing stocks of algal biomass carbon, and have Chl *a* concentrations that are more typical of oligotrophic waters. However, their thermokarst formation in carbon-rich permafrost soils and ongoing terrestrial organic matter inputs likely result in continuously large supplies of allochthonous carbon substrates for bacterial decomposition and oxygen demand and thus sets them apart from these other shallow lakes.

Oxygen-depleted water columns under the ice have been reported in thaw lakes elsewhere, for example over 2 months in Alaska thermokarst ponds (Fig. 5 in Clilverd et al. 2009), and prolonged under-ice anoxia may be a general feature of thermokarst aquatic ecosystems. Such conditions would be conducive to long periods of methanogenesis, consistent with the high methane concentrations measured in this study (Table 1), and the high rates of methane production reported in thaw lake studies elsewhere, including under the ice (e.g., Langer et al. 2015).

Under-ice changes in specific conductivity

The increased conductivity observed during winter in the subarctic thaw lakes is likely in part due to the exclusion of major ions from the ice during freeze-up, which is well known for polar lake waters; e.g., Welch and Bergmann (1985b) and Belzile et al. (2002). The increase in the near-bottom waters may also be due to bacterial mineralisation processes and the release of ions such as bicarbonate at the sediment-water interface. For example, Mortimer and Mackereth (1958) demonstrated that warming of bottom sediments combined with bacterial decomposition and ion release modifies the density structure of lakes under ice and creates gravity currents that move downslope. Given the bacterial respiration during this process, these gravity currents would be depleted in oxygen. Welch and Bergmann (1985b) indicated that the formation of gravity currents due to sediment mineralisation would cause the gravity currents from cryoconcentration to follow a similar flow path; i.e., the waters enriched in salts would flow from the margins of the lakes into the deepest regions. Terzhevik et al. (2009) verified the prediction that oxygen-depleted waters would flow along the lake margins, with the most O_2-depleted waters accumulating at depth.

We assessed whether cryoconcentration and respiration contributed to the increased specific conductivity in our study lakes by computing the increases that would occur by these processes. The observed temperature of 0°C in the upper 0.6 m of BGR1 indicated that the lake froze to that depth. From bathymetric data (V. Proult, Université Laval, unpubl. data), we compute that 49% of the total volume of water in BGR1 froze. The ions expelled from ice formation, assuming that all salts were excluded from ice (Pieters and Lawrence 2009), would therefore explain a doubling of specific conductivity in the remaining water column, to 195 μS cm^{-1}. Given the rate of oxygen depletion and the duration of winter ice cover, and following the stoichiometry of Mortimer and Mackereth (1958), we estimate that ~216 μS cm^{-1}

accumulated in BGR1 as a result of ion release from bacterial mineralisation processes. From fall to just before spring mixing, the specific conductivity at 3.5 m increased by 323 μS cm^{-1}, which could be accounted for by these two within lake processes, rather than external sources (Osterkamp 1987). Additional oxygen and conductivity sensors would be required to more accurately assess the flow paths of the water and the contribution of local respiration and advection to the changes at each depth.

The increased specific conductivity from cryoconcentration and sediment respiration led to salt-induced increases in density with depth, which in turn explain some of the unusual observations. For example, the near bottom temperatures were warmer than 5°C shortly after ice off in SAS2A and KWK12, and these were only possible due to the stabilizing increases in salt content of the lower water column. The more rapid increase in specific conductivity initially after ice formation and the slower increase after mid-December at 3.5 m suggest a time-dependent contribution of sediment respiration and cryoconcentration to salt concentration. Differing rates of these processes and the ensuing gravity currents may have contributed to the development of the mid-water-column temperature maximum demonstrated by U-shaped isotherms in early January in BGR1 (Fig. 3). Based on the earlier studies and our observation that the largest increases in specific conductivity over winter occurred at the depths of our deepest thermistors, we conclude that the rates of oxygen depletion in the lower water column resulted from local respiration and advection.

Mixing dynamics in spring and fall

In contrast to other dimictic subarctic lakes, the water column did not fully ventilate during mixing in spring and fall (Figs. 4-6). Due to the combination of cryoconcentration, respiration, and the likely generation of gravity currents, specific conductivity increased with depth over the winter with the largest increase in near bottom waters. The increased major ions induced stable stratification over the winter, where, on the basis of temperature alone, the water column would have mixed by late winter (Supporting Information Fig. S1). The production of low salinity water by melting ice in spring would have further contributed to the density gradient and stabilization of the water column at that time. The density gradient combined with high solar radiation reduced the potential for the lakes to mix fully by convection as is typically expected at ice-off. The persistence of the density difference over the summer reduced the efficacy of fall mixing. Mixing by heat loss may have been abetted by cloudy conditions in spring and reduced solar radiation coupled by decreasing air temperatures in fall (Figs. 5, 6).

Internal wave induced mixing is generally not expected in lakes only a tenth of a hectare in size, however the low Wedderburn numbers for BGR1 in spring indicated the potential for such mixing, and the step-like decreases in conductivity in the lower water column are consistent with such effects (Fig. 4). The distance between our study sites and the sites where winds were measured precludes exact values for Wedderburn numbers, but the abrupt increases and decreases in temperature, oxygen, or conductivity in the time series records for each of the lakes associated with recorded wind events (Figs. 3-6) support our interpretations. The temporal correlation in the changes of the three variables in SAS2A in late May to early June (Fig. 5) indicates that the sensors were located where gradients were present, as required for internal wave-induced motions to be seen. The extreme fluctuations in oxygen that were recorded in the mid-water column of KWK12 in early summer 2014, with values changing from anoxia to around 80% equilibrium, and back to anoxia over the course of 24 h are further evidence for internal wave motions (Fig. 7). These fluctuations were too large to be caused by biological processes and were synchronized with diurnal variations in the wind field suggesting wind-forced internal waves as opposed to seiches, whose period is 0.5 h. The more rapid ventilation of the water column of BGR1 at 1 m and the progressively later and only partial ventilation at greater depths imply that convective and internal wave induced mixing were operative in the upper water column during spring with internal wave motions more important deeper in the lake. No periods of complete mixing occurred in KWK12 or SAS2A following spring thaw (Figs. 5, 6, Supporting Information S2, S3). Thus, the combination of processes under the ice that led to strong density differences reduced the potential for spring mixing, and thereby would have retained dissolved greenhouse gases within the lakes as well as reduced the extent of reoxygenation.

Mixing was more vigorous and complete in fall relative to spring, and all three lakes showed a substantial degree of oxygenation over the period September–October. Winds increased on synoptic time scales and were higher than in the summer period (Figs. 4-6). During fall in BGR1, the Wedderburn number varied between 10 and 0.01, indicating the potential for several events that would have caused the thermocline to upwell and downwell with concomitant increased shear in the stratified waters. Prolonged surface water cooling at this time of year abetted by increased cloud cover and the seasonally induced decrease in solar radiation likely generated convective mixing. In all three lakes, the greatly increased oxygen concentrations beginning in September are indicative of mixing to depth. The higher frequency fluctuations are indicative of internal wave activity. Convective cooling and strong winds would have increased the gas transfer coefficient and enabled gas exchange with the atmosphere in both directions: the absorption of atmospheric oxygen by the water column and the venting of deep water CO_2 and CH_4 to the atmosphere. These conditions contrasted strongly with those in spring, when rapid warming combined with the solute density gradient likely

stabilised the water column and prevented full mixing and gas exchange.

The close alignment of the O_2 records in SAS2A (1.0 m, Fig. 5) and KWK12 (2.5 m, Fig. 6) during fall, despite the 17 km distance that separates them, indicates the importance of regional weather conditions in controlling their mixing dynamics. The concurrence of stratification and mixing processes in these two lakes also implies that persistent anoxia and similar mixing dynamics are likely to be observed amongst the multitudinous thaw lakes and ponds across this permafrost landscape.

Biogeochemical implications

The large changes in oxygen documented here imply that thaw lakes are highly reactive biogeochemical systems. Irrespective of permafrost regime, the three water bodies were supersaturated in CH_4 and CO_2, indicating that they are active sites of methanogenesis and microbial decomposition of organic matter, as has been observed similar to observations in other thaw lakes (e.g., Walter et al. 2006). Several features of the oxygen regime are likely to favor these biogeochemical processes. Prolonged anoxia will be conducive to anaerobic processes including methanogenesis, while the presence of aerobic conditions in the surface waters will favor methanotrophs and their oxidation of CH_4 diffusing up from the anoxic waters and sediments below (Crevecoeur et al. 2015). The alternation of aerobic and anaerobic conditions through time may be especially conducive to the breakdown of complex organics derived from ancient terrigenous sources. Photochemistry may additionally aid this process by converting CDOM into low molecular weight compounds (Laurion and Mladenov 2013; Cory et al. 2014). The high concentrations of greenhouse gases in these lakes indicate that fluxes to the atmosphere could be considerable (Laurion et al. 2010). Ventilation of the lower water column was greatest in fall, however mixing was incomplete, even during this period. The quantity of gases which evade may vary between years, with greatest evasion in the years that experience the highest winds in fall.

Conclusions

The high frequency measurements obtained in this study revealed many features of permafrost thaw lakes that differentiate them from other lakes and that were not apparent from intermittent water column profiling. Despite their shallow depth, thaw lakes were strongly stratified through most of the year, and cryoconcentration and respiration intensified their density stratification under the ice. Unlike shallow hypereutrophic lakes in which internally produced (autochthonous) organic carbon provides the substrate for respiration and oxygen drawdown, the organic matter in thaw lakes results from their thermokarst formation in carbon-containing tundra soils and from additional external loading from the landscape. In spring, mixing was incomplete due to the strong density gradient that formed during winter, and this precluded the full water column mixing that is characteristic of most dimictic lakes. Despite their small size, internal wave motions were present and likely contributed to mixing. In fall, the water column mixed more extensively but not fully. Anoxic conditions were prevalent throughout much of winter as the result of initial high rates of oxygen loss combined with a small volume in these organic-rich systems. Thus, physical and biogeochemical processes under the ice cause strong density stratification, which coupled with the high respiratory oxygen demand cause thaw lakes to be anoxic systems throughout much of the year. Periods in which mixing oxygenates the water column, even partially, favor intensified rates of aerobic processes. Subarctic thaw lakes and ponds, a major class of freshwater ecosystems in the circumpolar north, operate for most of the year as anoxic bioreactors that are likely to be highly conducive to anaerobic microbial processes such as methane production.

References

Allard, M., and M. K. Seguin. 1987. The Holocene evolution of permafrost near the tree line, on the eastern coast of Hudson Bay (northern Quebec). Can. J. Earth Sci. **24**: 2206–2222. doi:10.1139/e87-209

AMAP. 2012. Arctic Climate Issues 2011: Changes in Arctic Snow, Water, Ice and Permafrost. SWIPA 2011 Overview Report.

Amorocho, J., and J. J. DeVries. 1980. A new evaluation of the wind stress coefficient over water surfaces. J. Geophys. Res. **85**: 433–442. doi:10.1029/JC085iC01p00433

Baird, D. J., T. E. Gates, and R.W. Davies. 1987. Oxygen conditions in two prairie pothole lakes during winter ice cover. Can. J. Fish. Aquat. Sci. **44**: 1092–1095. doi:10.1139/f87-131

Barica, J., and J. A. Mathias. 1979. Oxygen depletion and winterkill risk in small prairie lakes under extended ice cover. J. Fish. Res. Board Can. **36**: 980–986. doi:10.1139/f79-136

Belzile, C., J. Gilson, and W. F. Vincent. 2002. Colored dissolved organic matter and dissolved organic carbon exclusion from lake ice: Implications for irradiance transmission and carbon cycling. Limnol. Oceanogr. **47**: 1283–1293. doi:10.4319/lo.2002.47.5.1283

Bhiry, N., and others. 2011. Environmental change in the Great Whale River region, Hudson Bay: Five decades of multidisciplinary research by Centre d'études nordiques (CEN). Ecoscience **18**: 182–203. doi:10.2980/18-3-3469

Bouchard, F., P. Francus, R. Pienitz, I. Laurion, and S. Feyte. 2014. Subarctic thermokarst ponds: Investigating recent landscape evolution and sediment dynamics in thawed permafrost of Northern Québec (Canada). Arct. Antarct. Alp. Res. **46**: 251–271. doi:10.1657/1938-4246-46.1.251

Breton, J., C. Vallières, and I. Laurion. 2009. Limnological properties of permafrost thaw ponds in northeastern

Canada. Can. J. Fish. Aquat. Sci. **66**: 1635–1648. doi:10.1139/F09-108

Calmels, F., and M. Allard. 2004. Ice segregation and gas distribution in permafrost using tomodensitometric analysis. Permafrost Periglac. **15**: 367–378. doi:10.1002/ppp.508

CEN. 2014a. Climate station data from the Umiujaq region in Nunavik, Quebec, Canada, v. 1.1 (1997–2013). Nordicana **D9**. doi:10.5885/45120SL-067305A53E914AF0

CEN. 2014b. Climate station data from the Whapmagoostui-Kuujjuarapik Region in Nunavik, Quebec, Canada, v. 1.2 (1987–2013). Nordicana **D4**. doi:10.5885/45057SL-EADE4434146946A7

Chen, C.-T., and F. J. Millero. 1977. The use and misuse of pure water PVT properties for lake waters. Nature **266**: 707–708. doi:10.1038/266707a0

Clilverd, H., D. White, and M. Lilly. 2009. Chemical and physical controls on the oxygen regime of ice-covered Arctic lakes and reservoirs. J. Am. Water Resour. Assoc. **45**: 500–511. doi:10.1111/j.1752-1688.2009.00305.x

Cory, R. M., C. P. Ward, B. C. Crump, and G. W. Kling. 2014. Sunlight controls water column processing of carbon in arctic fresh waters. Science **345**: 925–928. doi:10.1126/science.1253119

Crevecoeur, S., W. F. Vincent, J. Comte, and C. Lovejoy. 2015. Bacterial community structure across environmental gradients in permafrost thaw ponds: Methanotroph-rich ecosystems. Front. Microbiol. **6**: 192. doi:10.3389/fmicb.2015.00192

Downing, J. A. 2009. Global limnology: Up-scaling aquatic services and processes to planet Earth. Verh. Internat. Verein. Limnol. **30**: 1149–1166.

Elberling, B., and others. 2013. Long-term CO_2 production following permafrost thaw. Nat. Clim. Chang. **3**: 890–894. doi:10.1038/nclimate1955

Grosse, G., B. Jones, and C. Arp. 2013. Thermokarst lakes, drainage, and drained basins, p. 325–353. *In* J. Shroder, R. Giardino and J. Harbor [eds.], Treatise on geomorphology. Academic Press.

Hobbie, J. E. 1980. Limnology of tundra ponds, Barrow Alaska Dowden. Hutchinson & Ross.

Hutchinson, G. E. 1957. A treatise on limnology. Wiley.

Imberger, J., and J. C. Patterson. 1990. Physical limnology. Adv. Appl. Mech. **27**: 303–473. doi:10.1016/S0065-2156(08)70199-6

Kalff, J. 2002. Limnology. Prentice Hall.

Kirillin, G., and others. 2012. Physics of seasonally ice-covered lakes: A review. Aquat. Sci. **74**: 1015–1621. doi:10.1007/s00027-012-0279-y

Langer, M., S. Westermann, K. Walter-Anthony, K. Wischnewski, and J. Boike. 2015. Frozen ponds: Production and storage of methane during the Arctic winter in a lowland tundra landscape in northern Siberia, Lena River delta. Biogeosciences **12**: 977–990. doi:10.5194/bg-12-977-2015

Laurion, I., and N. Mladenov. 2013. Dissolved organic matter photolysis in Canadian arctic thaw ponds. Environ. Res. Lett. **8**: 035026. doi:10.1088/1748-9326/8/3/035026

Laurion, I., W. F. Vincent, S. MacIntyre, L. Retamal, C. Dupont, P. Francus, and R. Pienitz. 2010. Variability in greenhouse gas emissions from permafrost thaw ponds. Limnol. Oceanogr. **55**: 115–133. doi:10.4319/lo.2010.55.1.0115

MacIntyre, S., J. P. Fram, P. J. Kushner, N. D. Bettez, W. J. O'Brien, J. E. Hobbie, and G. W. Kling. 2009. Climate-related variations in mixing dynamics in an Alaskan arctic lake. Limnol. Oceanogr. **54**: 2401–2417. doi:10.4319/lo.2009.54.6_part_2.2401

McGuire, A. D., and others. 2012. An assessment of the carbon balance of Arctic tundra: Comparisons among observations, process models, and atmospheric inversions. Biogeosciences **9**: 3185–3204. doi:10.5194/bg-9-3185-2012

Mortimer, C. H., and F. J. H. Mackereth. 1958. Convection and its consequences in ice-covered lakes. Verh. Internat. Ver. Limnol. **13**: 923–932.

Osterkamp, T. E. 1987. Freezing and thawing of soils and permafrost containing unfrozen water or brine. Water Resour. Res. **23**: 2279–2285. doi:10.1029/WR023i012p02279

Pawlowicz, R. 2008. Calculating the conductivity of natural waters. Limnol. Oceanogr.: Methods **6**: 489–501. doi:10.4319/lom.2008.6.489

Pieters, R., and G. A. Lawrence. 2009. Effect of salt exclusion from lake ice on seasonal circulation. Limnol. Oceanogr. **54**: 401–412. doi:10.4319/lo.2009.54.2.0401

Ramlal, P. S., R. H. Hesslein, R. E. Hecky, E. J. Fee, J. W. M. Rudd, and S. J. Guildford. 1994. The organic carbon budget of a shallow Arctic tundra lake on the Tuktoyaktuk Peninsula, N.W.T., Canada. Biogeochemistry **24**: 145–172. doi:10.1007/BF00003270

Schindler, D. W., H. E. Welch, J. Kalff, G. J. Brunskill, and N. Kritsch. 1974. Physical and chemical limnology of Char Lake, Cornwallis Island (75° N lat.). J. Fish. Res. Board Can. **31**: 585–607. doi:10.1139/f74-092

Schuur, E. A. G., and others. 2015. Climate change and the permafrost carbon feedback. Nature **520**: 171–179. doi:10.1038/nature14338

Terzhevik, A., and others. 2009. Some features of the thermal and dissolved oxygen structure in boreal, shallow ice-covered Lake Vendyurskoe, Russia. Aquat. Ecol. **43**: 617–627. doi:10.1007/s10452-009-9288-x

Thibault, S., and S. Payette. 2009. Recent permafrost degradation in bogs of the James Bay area, Northern Quebec, Canada. Permafrost Periglac. **20**: 383–389. doi:10.1002/ppp.660

Verpoorter, C., T. Kutser, D. A. Seekell, and L. J. Tranvik. 2014. A global inventory of lakes based on high-resolution satellite imagery. Geophys. Res. Lett. **41**: 6396–6402. doi:10.1002/2014GL060641

Vincent, W. F., I. Laurion, R. Pienitz, and K. M. Walter-Anthony. 2013. Climate impacts on arctic lake ecosystems, p. 27–42. *In* C. R. Goldman, M. Kumagai and R. D. Robarts [eds.], Climate change and global warming of inland waters: Impacts and mitigation for ecosystems and societies. Wiley.

Walter, K. M., S. A. Zimov, J. P. Chanton, D. Verbyla, and F. S. Chapin, III. 2006. Methane bubbling from Siberian thaw lakes as a positive feedback to climate warming. Nature **443**: 71–75. doi:10.1038/nature05040

Watanabe, S., I. Laurion, K. Chokmani, R. Pienitz, and W. F. Vincent. 2011. Optical diversity of thaw ponds in discontinuous permafrost: A model system for water color analysis. J. Geophys. Res. **116**: G02003. doi:10.1029/2010JG001380

Welch, H. E. 1974. Metabolic rates of arctic lakes. Limnol. Oceanogr. **19**: 65–73. doi:10.4319/lo.1974.19.1.0065

Welch, H. E., and M. A. Bergmann. 1985a. Winter respiration of lakes at Saqvaqjuac, N.W.T. Can. J. Fish. Aquat. Sci. **42**: 521–528. doi:10.1139/f85-069

Welch, H. E., and M. A. Bergmann. 1985b. Water circulation in small arctic lakes in winter. Can. J. Fish. Aquat. Sci. **42**: 506–520. doi:10.1139/f85-068

Welch, H. E., P. J. Dillon, and A. Sreedharan. 1976. Factors affecting winter respiration in Ontario lakes. J. Fish. Res. Board Can. **33**: 1809–1815. doi:10.1139/f76-232

Whalen, S. C., and J. C. Cornwell. 1985. Nitrogen, phosphorus, and organic carbon cycling in an Arctic lake. Can. J. Fish. Aquat. Sci. **42**: 797–808. doi:10.1139/f85-102

Acknowledgments

We thank P. Bégin, J. Comte, S. Crevecoeur, A. Przytulska-Bartosiewicz, F. Bouchard, and C. Tremblay for their help in the field, D. Sarrazin for advice and helpful discussions regarding field instrumentation, I. Laurion for continued feedback and guidance, M. Lionard and M.-J. Martineau for laboratory support, and A. Crowe for programming assistance. This study was made possible with financial support from the Natural Sciences and Engineering Research Council of Canada (NSERC), the Canada Research Chair program, the Quebec nature and technology research funds (FRQNT), and U.S. National Science Foundation Grants DEB 0919603 and ARC 1204267 to SM. Financial and logistical support were further provided by the Centre for Northern Studies (CEN, Université Laval), the ADAPT (Arctic Development and Adaptation to Permafrost in Transition) Discovery Frontiers grant, and the Northern Science Training Program.

Submitted 19 December 2014
Revised 18 May 2015
Accepted 22 May 2015

Associate editor: John Downing